Test Observations of the Kyoto Tridimensional Spectrograph II at University of Hawaii 88-inch and Subaru Telescopes

H. Sugai[a], T. Hattori[b], A. Kawai[a], S. Ozaki[c], G. Kosugi[d], H. Ohtani[e], T. Hayashi[f],
T. Ishigaki[g], M. Ishii[h], M. Sasaki[i], A. Shimono[a], Y. Okita[a], J. Sudo[a], N. Takeyama[j]

[a]Department of Astronomy, Kyoto University, Kitashirakawa, Sakyo-ku, Kyoto 606-8502,
Japan

[b]Okayama Astrophysical Observatory, National Astronomical Observatory of Japan,
Kamogata-cho, Asakuchi-gun, Okayama 719-0232, Japan

[c]Nishiharima Observatory, Nishikawauchi 407-2, Sayo-cho, Sayo-gun, Hyogo 679-5313, Japan

[d]Subaru Telescope, National Astronomical Observatory of Japan, 650 North A'Ohoku Place,
Hilo, Hawaii 96720, U.S.A.

[e]Ryukoku University, Tsukamoto-cho 67, Fukakusa, Fushimi-ku, Kyoto 612-8577, Japan

[f]Toyama Science Museum, Nishinakanocho 1-18-31, Toyama-shi, Toyama 939-8084, Japan

[g] Department of Applied Physics, Graduate School of Engineering, Hokkaido University,
Kita-ku, Sapporo 060-8628, Japan

[h]Kurashiki Science Center, Furushinden 940, Fukuda, Kurashiki-shi, Okayama 712-8046,
Japan

[i]Shimonoseki City University, Shimonoseki, Yamaguchi 751-8510, Japan

[j]Genesia Corporation, Shimorenjaku 3-38-4, Mitaka-shi, Tokyo 181-0013, Japan

ABSTRACT

In order to investigate the physical conditions of ionized gas in galaxies, as well as its kinematics, we have developed the Kyoto tridimensional spectrograph II (3DII). It is a multi-mode instrument designed for Cassegrain focus, including integral field spectrograph (IFS) and Fabry-Perot imager modes. We have designed it compact so that we can mount it at 2-m class telescopes as well as at 8-m Subaru telescope.

We have succeeded in test observations of the 3DII. In the IFS mode the spatial resolution of $\sim 0''.5$ and $0''.4$ was obtained in 30-minute exposures at University of Hawaii 88-inch (UH88) and Subaru, respectively, in relatively good weather conditions. Each of 37×37 microlenses subtends $\sim 0''.1$ in Subaru's case. This samples well the image size. A wider field of view is emphasized in the case of UH88. Because our micropupil spectroscopy is free from a slit effect, we have reached the accuracy of an order of one tenth of a pixel for deriving velocity fields in terms of velocity center while the full width at half maximum of the instrumental profile corresponds to two pixels. At Subaru we have used a container designed in a collaboration with National Astronomical Observatory, Japan: it fits with a robotic instrument exchanger. The container includes two heat exchangers to keep its surface cool and avoid degrading the image quality. We have established effective observational sequences by realizing a software interface with Subaru operating system. Some results from target observations are shown.

Keywords: Tridimensional multimode spectrograph, Integral field spectrograph, Microlens array, Fabry-Perot, UH88, Subaru

---

1. INTRODUCTION

The Kyoto tridimensional spectrograph II[1,2] (3DII) is the second version of the Kyoto tridimensional spectrograph I[3] (3DI), which has been successfully operated at the Okayama 1.9m telescope in Japan. The 3DII has four observational modes: integral field spectrograph (IFS) with a microlens array, Fabry-Perot (FP) imager, long-slit spectrograph, and filter-imaging modes. The IFS mode is a similar type to that developed by Bacon et al.[4] The 3DII is so far the only spectrograph with FP and/or IFS modes that has been mounted or is planned to be mounted on Subaru telescope. The optics is designed to be used in wide wavelength ranges from 360 nm to 900 nm.

We succeeded in the 3DII test observations[5] at a 1.5m "Subaru simulator" telescope at Mitaka in Tokyo on May 27-June 5, 2000. After this success, application was submitted for mounting the 3DII at Subaru as a PI-type instrument. A technical report and a report of intermediate-timescale scientific goals were evaluated by separate committees. We have mounted our spectrograph on University of Hawaii 88-inch telescope (UH88) in June, 2002, and on Subaru in August, 2002 (Figure 1). Although results of the test observations at Subaru are mainly described in this paper, consistent results were obtained at the UH88 as well as at the "simulator" telescope. The observing parameters for each mode are shown in Table 1.

Table 1. Observing Parameters

OBSERVATIONAL MODE	ON SUBARU (8.2 m, F/12.2)	ON UH88 (2.22 m, F/10.14)
Fabry-Perot	$0''.056$ pixel^{-1} [a] Field of view $1'.9 \times 1'.9$[b] (Velocity shift Δv (km s^{-1}) $= 980 \times (\theta')^2$) $R \equiv \lambda/\Delta\lambda \sim 400$ and 7000 $(400 - 700$ nm$)$[c]	$0''.25$ pixel^{-1} Field of view $8'.5 \times 8'.5$ $(\Delta v$ (km s^{-1}) $= 49.5 \times (\theta')^2)$
Integral field spectrograph with a microlens array	$0''.093$ lens^{-1} Field of view $3''.4 \times 3''.4$ Number of spectra $\simeq 1000$ $R \simeq 1200$ $(360 - 900$ nm$)$[d,e]	$0''.42$ lens^{-1} Field of view $15'' \times 15''$
Long slit	Width $0''.12$, $0''.19$, $0''.56$ or Width $0''.17$, $0''.62$, $2''.1$ Length $1'.5$ $R \simeq 1200$ for $0''.12$ slit[d]	Width $0''.55$, $0''.83$, $2''.5$ or Width $0''.78$, $2''.8$, $9''.2$; Length $6'.7$ $R \simeq 1200$ for $0''.55$ slit
Narrow-band imaging	$0''.056$ pixel^{-1} Field of view $1'.9 \times 1'.9$	$0''.25$ pixel^{-1} Field of view $8'.5 \times 8'.5$

[a]We use binning (e.g., 2×2) before adaptive optics at optical wavelengths becomes available.

[b]In the FP mode, the wavelength with a peak transmission varies over the field of view. If we define an effective field of view as the field where the wavelength shift is smaller than one tenth of the wavelength resolution, it is $33''$ diameter on Subaru, without scanning, for the etalon with a spectral resolution of $R \simeq 400$. The angular distance θ arcmin is measured from a velocity center.

[c]Only an etalon with a lower spectral resolution was used in the test observations so far. A higher resolution one remains untested. Another Fabry-Perot etalon also will become available for a bluer wavelength region around 370 nm.

[d]A grism with higher spectral resolution $R \simeq 4000$ will become available.

[e]Only a part of the wavelength range between 360 and 900 nm is actually observed simultaneously: five grisms will cover the whole wavelength range.
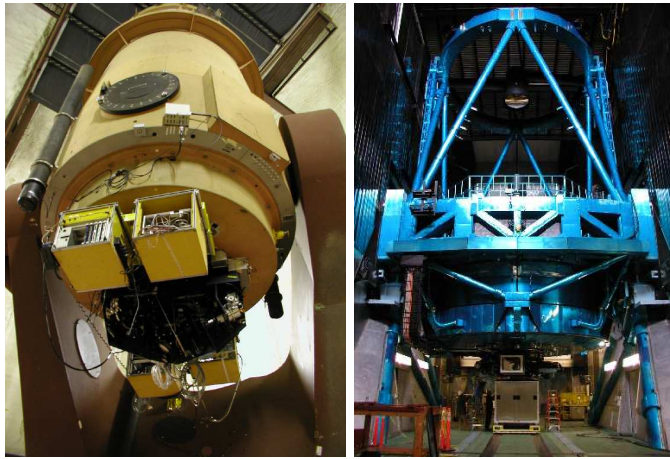
Figure 1. Kyoto 3DII mounted on University of Hawaii 88-inch telescope (left: June 5-9, 2002) and on Subaru telescope (right: August 26-28, 2002).

2. TARGET ACQUISITION IN IFS MODE

In order to acquire a target onto the microlens array, we take advantage of a wider field of view (FOV) of filter-imaging mode. Using a binning such as of 3×3 pixels, we quickly obtain a target image. Next we make a small adjustment for a telescope pointing to move the target on a certain position on CCD. When we change the filter-imaging mode into the IFS mode, we find the target at or close to the center of the IFS FOV. In the case that we need a further fine adjustment, we quickly reconstruct a target image in the IFS mode by using non-dispersed micropupil images, and make the corresponding adjustment for the telescope pointing.

3. FOCUSING & QUICK LOOK

We carry out focusing inside the 3DII with Hartmann test by using a mask within the instrument. The camera is focused for non-dispersed micropupils in the IFS mode, and for a slit position in the other modes, respectively.

In order to set a telescope focus onto a stellar image (on the microlens array for the IFS mode, and at the slit position for the other modes), we adjust the position of a telescope secondary mirror. In the case of the IFS mode at UH88, this is carried out by quickly reconstructing the stellar image from non-dispersed micropupil images (Figure 2). In the case of Subaru, it is enough to do this only once at the beginning of the run: for later refocusings, an offset of secondary mirror focus position between for a telescope guide star and for a target star of the instrument is applied after the refocusing of the guide star. In this way, we have realized a spatial resolution of $\sim 0''.4$ in 30-minute exposures when the seeing conditions are good (Section 13).

Right after a target exposure or during later exposures, it is possible to check the IFS data by quickly reconstructing images (Figure 3).

4. SCALING

For designing the 3DII, we have put weights on minimizing chromatic aberrations because it is used in wide wavelength regions. We instead gave some tolerance to distortion. It is therefore important to make a correction for the distortion in order to determine relative positions accurately in the FP, filter-imaging, and slit-spectroscopic modes, whose FOV's are large. In a laboratory, we made a preliminary experiment for this correction by taking advantage of accurate pitches among micropupil images[1] produced right behind a microlens array. By fitting a third-order polynomial to their refocused image positions on the CCD, we were able to correct the distortion to an accuracy of one fourth of a pixel. In actual observations of a globular cluster at Subaru, corrected relative positions of stars were consistent with their catalog positions within the catalog's uncertainties, $\sim 0''.05$-$0''.07$. The pixel scale at the FOV center has been measured as $0''.056$ pixel^{-1}, which is consistent with the design.

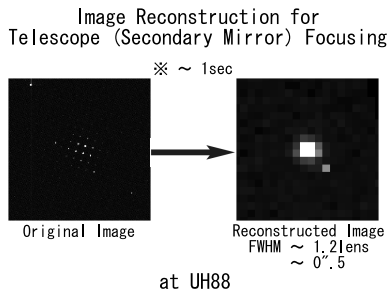Image Reconstruction for
Telescope (Secondary Mirror) Focusing

※ ~ 1sec

Original Image   Reconstructed Image
                        FWHM ~ 1.2lens
                            ~ 0″.5

at UH88

Figure 2. An example of image reconstruction for the focusing of a stellar image on a microlens array.

Quick Look (Image Reconstruction)

※ ~ 3 sec each

Continuum   [O Ⅲ]
(5100 Å)

at UH88
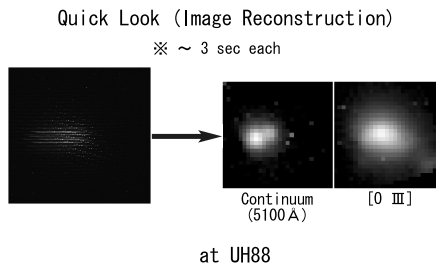
Figure 3. An example of image reconstruction for a quick look.

The distortion is negligible for the IFS mode since its FOV is much smaller. In order to measure the sampling scale at Subaru, we have observed a binary star whose separation is $1''.53$ ($\Sigma 3062$ Cas: 2002). The derived scaling of $0''.096$ lens^{-1} is larger than the designed scaling only by ~ 3 %, although this slight difference is not a problem at all. The difference is not caused by a microlens pitch, because the measured pitch[1] of 1.540 ± 0.002 mm (1σ among microlenses) was exactly as designed.

5. STABILITY OF MICROPUPIL IMAGE POSITIONS

In order to obtain accurate flat fielding and wavelength calibration for the IFS mode, the stability of the micropupil image positions is important. By combining ANSYS and Code V, we have designed the instrument so that the movements on the CCD of the light from the center of the focal plane are almost within one pixel for any telescope attitude. This has been confirmed during evaluation and test observations at a 1.5m telescope in Tokyo.[5] The stability also has been checked during test observations at Subaru in a more practical way. We obtained seven "long"-exposure (longer than 20 minutes) IFS frames. The average movement between a wavelength calibration frame which was taken before a long exposure and one which was taken after it was 0.05 pixel (0.13 pixel in the worst case) in dispersion direction and 0.12 pixel (0.23 pixel at worst) in its vertical direction. This included the reproducibility of a mirror position for a calibration lamp. The movement of 0.05 pixel in dispersion direction corresponds to only one fortieth of a velocity resolution.

6. POINT SPREAD FUNCTION

In a laboratory, we measured point spread functions for the filter-imaging mode by setting a pinhole at the focal plane in a laboratory and by moving around the pinhole within the plane. The measured sizes of the pinhole image were one pixel or so, as designed. During test observations at Subaru and UH88, the obtained point spread functions were limited not by the instrument optics but by the seeing ($0''.4$- $0''.5$ at best), as expected. Similarly, point spread functions for the IFS mode were limited by the seeing ($0''.4$ at best).

7. EFFICIENCY

Figure 4 shows the measured efficiencies for all modes in the 3DII: filter-imaging, FP, slit-spectroscopic, and IFS modes. The efficiencies include all the optical elements in the instrument, such as the throughputs of lenses, mirrors, filters, and an FP/MLA, and the quantum efficiency of the CCD. They also include the telescope (+ADC) and atmospheric transmissions. We now run the 3DII with single-layer anti-reflection coated lenses, and the efficiencies are roughly consistent with the expected ones. In order to improve them further, we are planning to replace these lenses with multi-layer, anti-reflection coated ones in future.

8. DETECTOR & REFRIGERATOR

We use an anti-reflection coated backside-illuminated $2K \times 2K$ CCD, made by EEV, in order to achieve high efficiency at short wavelengths. For the CCD control and data acquisition, we use the improved fourth version of MESSIA[6] (modularized expandable system for image acquisition). This system is based on VMEbus, which is connected to Sbus in a workstation through optical fibers. The readout noise has been measured as $\sim$ 6-8 e^-, with a gain of 1.3 e^- ADU^{-1}. After a hardware binning of pixels, the readout noise was the same for the binned "pixel". The CCD dewar is cooled by a Stirling-cycle refrigerator. We have controlled the CCD temperature at ~ -100 °C, so that the detector has only negligible dark current, $\sim 10^{-3}$ e^- s^{-1} pixel^{-1}.

9. SENSITIVITY

The measured sensitivities of the IFS ($R = 1200$) mode at Subaru are the followings:

$(3\sigma$ **per** $0''.093 \times 0''.093$ **lens** per 2 wavelength pixels in 30min)

$\sim 7 \times 10^{-17}$ erg s^{-1} cm^{-2} Å^{-1} arcsec^{-2} at 5000 Å

$\sim 5 \times 10^{-17}$ erg s^{-1} cm^{-2} Å^{-1} arcsec^{-2} at 6600 Å

The sensitivities are similar to expected ones, since the efficiencies and noises are similar to expected ones. The moon, whose brighter side had an areal fraction of ~ 0.8 during the test observations, did not degrade the above sensitivities when the moon was farther than 20°-40° from a target object.

The measured sensitivities of the FP mode for line emission are the followings:

$R \sim 200$ at 5500 Å

$(3\sigma$ **per** $0''.11 \times 0''.11$ **(i.e.,**2×2**-binned) "pixel"** in 30min)

$\sim 1.2 \times 10^{-16}$ erg s^{-1} cm^{-2} arcsec^{-2} at 5500 Å

$R \sim 250$ at 7000 Å

$(3\sigma$ **per** $0''.11 \times 0''.11$ **(i.e.,**2×2**-binned) "pixel"** in 30min)

$\sim 1.3 \times 10^{-16}$ erg s^{-1} cm^{-2} arcsec^{-2} at 7000 Å

The above FP sensitivities have been derived by assuming a dark sky whose brightness corresponds to 21.3 mag arcsec^{-2} in V band. Even in such a condition, sky background dominates the noise in a 30-minute exposure. The derived sensitivities are similar to expected ones.

10. INTERFACE TO SUBARU

We have collaborated with National Astronomical Observatory of Japan to design a container for the 3DII and a mechanical adapter which connects the instrument with the container.[2] The container can be used by other instrument groups once they make an adapter for their instrument. The container fits with a robotic instrument exchanger CIAX[7,8] (Cassegrain Instrument Auto eXchanger for the Subaru Telescope). We have not had any problem with the hardware interface between the 3DII, the adapter, and the container during test observations at Subaru as well as in tests at Subaru Cassegrain Simulators in Tokyo and in Hilo. We also have accomplished a software interface between the 3DII and Subaru observing system (SOS) through Subaru interface (SI). Observers control not only Subaru but also the 3DII with commands from SOS. This has enabled us to establish effective observing sequences. We have realized an observing efficiency (a fraction of time in which a shutter is open, compared with the total time) of more than 70% during target observations.
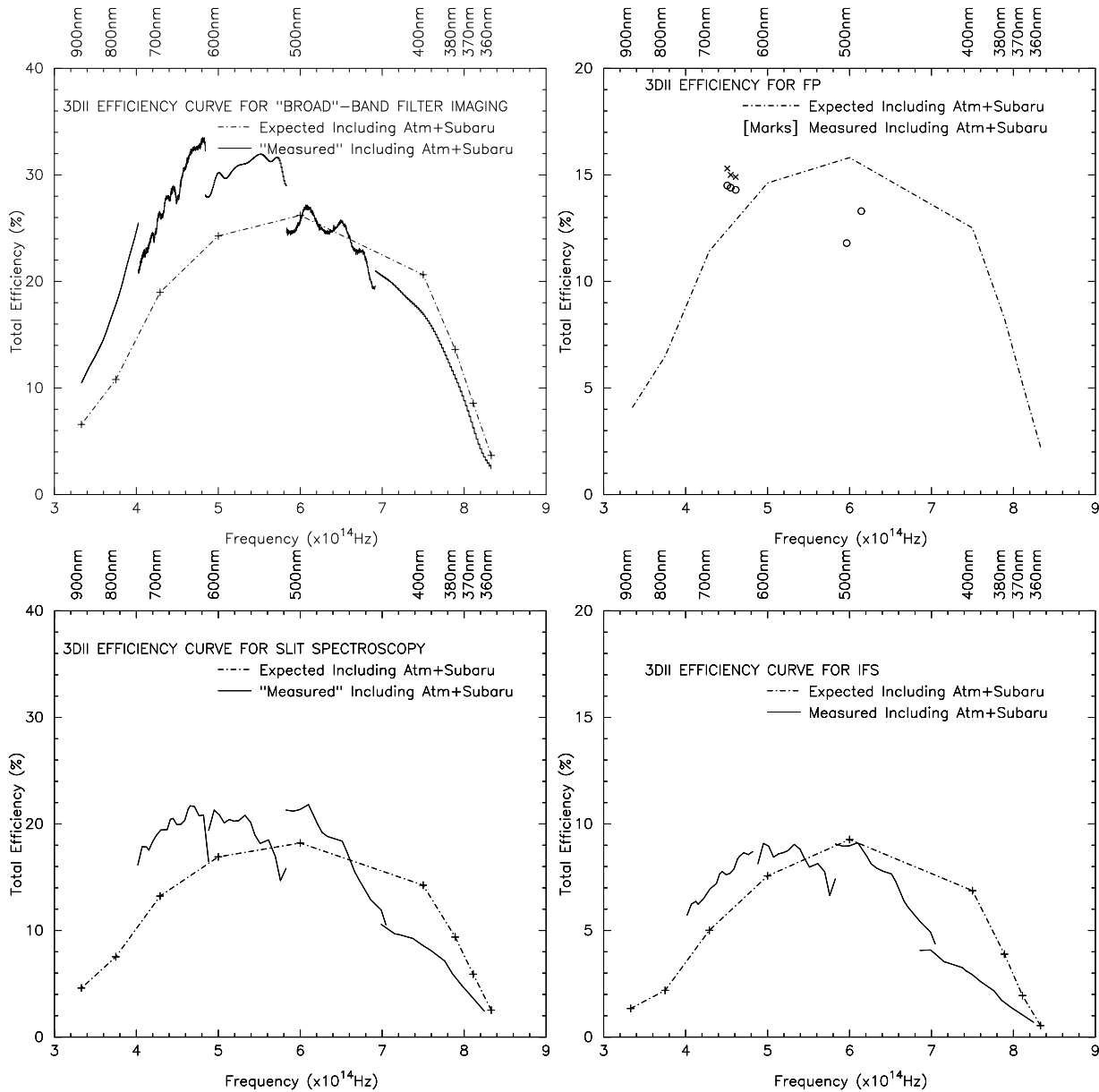
Figure 4. (upper left): Total efficiency for "Broad"-band filter imaging at Subaru. The shape of efficiency curve within each band was assumed, and its absolute value was obtained from the actual "broad"-band filter imaging data. The efficiency includes all the optical elements in the instrument and the quantum efficiency of the CCD. It also includes the telescope (+ADC) and atmospheric transmissions. The airmass of the observed standard star was 1.05. (upper right): Total efficiency for Fabry-Perot mode at Subaru. "o" marks are for one set of data for a standard star. "×" marks are for another set of the same star, which was obtained about ten minutes later. The difference between these two sets implies that the atmospheric transmittance might have not been perfect on these Fabry-Perot data. The efficiency at 5026 Å will be improved with a new order-sorting filter, which was not but is now available. The efficiency at 4880 Å may be only slightly affected by the Hβ absorption in the B1.5V star. The airmass of the star was 1.01. (lower left): Total efficiency for Slit spectroscopy at Subaru. The airmass of the observed standard star was 1.10. (lower right): Total efficiency for Integral Field Spectrograph mode at Subaru. The airmass of the observed standard star was 1.07.
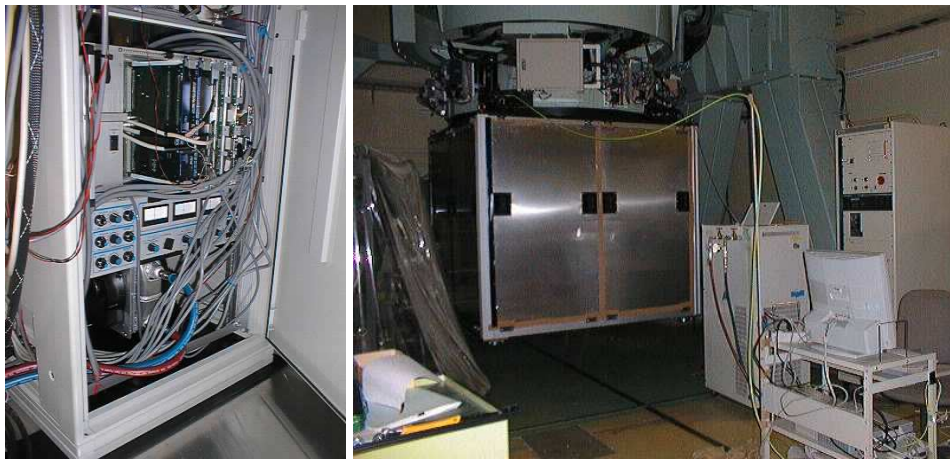
Figure 5. Heat control tests at Subaru Cassegrain Simulator in Mitaka, Tokyo. (left): We place a heat exchanger inside the controller rack. Another exchanger is placed outside the rack but within a container. (right): Cooling water with temperature of $\sim 3°$C lower than the air outside a container is supplied at 5.7 litter per minute. The temperature of outer surface of the container walls was kept almost at the same as or slightly lower than the air temperature. Similar results have been obtained at Subaru.

11. HEAT CONTROL

In the case of Subaru, the instrument as well as its controller rack are placed inside a container. We have designed heat control within the container so that the effect of heat transfer through natural convection between the outer surface of the container and the air inside the dome is negligible compared with the tolerance level of dome seeing, $0''.12$. In order to achieve this, we have used two heat exchangers: one inside the controller rack and the other outside it but within the container. Moreover, we have closed the container with walls made by heat insulators.

Figure 5 shows heat control tests carried out at Subaru Cassegrain Simulator in Mitaka, Tokyo. We have found that the temperature of outer surface of the walls is kept almost at the same as or slightly lower (by 0.1-$0.2°$C) than the air temperature outside the container. Therefore, the image quality is not degraded. The similar results have been actually obtained during test observations at Subaru.

12. REDUCTION SOFTWARE

We have developed a reduction software for the IFS mode. Procedures special to this mode are run with programs written in C language. Figure 6 shows as an example the extraction of spectra, which is based on Halogen lamp spectra. Standard procedures, such as wavelength and flux calibration, are run by using IRAF tasks and scripts. In either case, all procedures are carried out automatically.

13. EXAMPLE OF OBSERVATIONAL RESULTS

In order to establish effective observational sequences (see Section 10), we have actually observed some target objects. Figures 7, 8, 9, and 10 show some results for a Seyfert galaxy in the IFS mode at Subaru. Figure 7 shows the "observed" spatial distribution of the broad component of the Hα emission, which should be a point source. This figure indicates that the spatial resolution in this 30-minute exposure was $\sim 0''.4$. In Figure 8, the nuclear component is clearly separated from a starburst ring/mini-spiral in the narrow component of the Hα emission. Its velocity structure is clearly seen even within one velocity resolution of ~ 250 km s^{-1}. Figures 9 and 10 show the spatial variations of line ratios and are indicative of physical conditions of the ionized gas. High spatial sampling matches well with Subaru's excellent image quality.
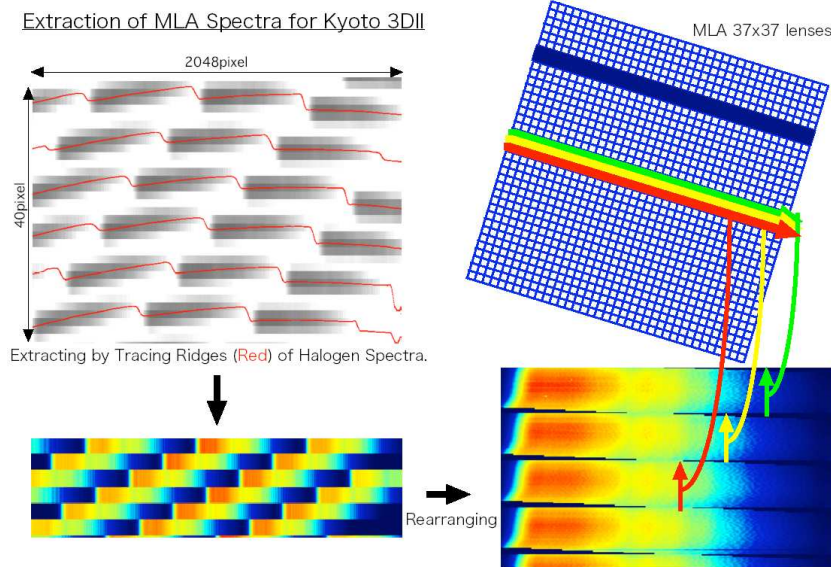
Figure 6. A part of automated reduction software.

Both at Subaru and UH88, we have succeeded in test observations in the IFS and FP modes as well as more "standard" modes including filter-imaging and slit spectroscopic modes. After these test observations, we have applied for and succeeded in obtaining observing time at Subaru as open use programs. The 3DII is ready for obtaining the unique data cube with a high spatial resolution at Subaru, and with a wider spatial extent at UH88.

ACKNOWLEDGMENTS

REFERENCES

1. H. Sugai *et al.*, "Kyoto tridimensional spectrograph II," *Proc. SPIE* **3355**, pp. 665–674, 1998.
2. H. Sugai *et al.*, "Kyoto tridimensional spectrograph II: progress," *Proc. SPIE* **4008**, pp. 558–569, 2000.
3. H. Ohtani *et al.*, "Kyoto tridimensional spectrograph I," *Proc. SPIE* **3355**, pp. 750–761, 1998.
4. R. Bacon *et al.*, "3D spectrography at high spatial resolution. I. concept and realization of the integral field spectrograph TIGER.," *Astron. Astrophys. Suppl. Ser.* **113**, pp. 347–357, 1995.
5. H. Sugai, S. Ozaki, T. Hattori, and A. Kawai, "The Kyoto tridimensional spectrograph II: evaluation at 1.5m 'Subaru simulator' telescope," in *Galaxies: The Third Dimension*, M. Rosado, L. Binette, and L. Arias, eds., *Astron. Soc. Pacif. Conf. Ser.* **282**, pp. 433–440, Astronomical Society of the Pacific, (San Francisco), 2002.
6. M. Sekiguchi, H. Iwashita, M. Doi, N. Kashikawa, and S. Okamura, "Development of a 2000 × 8144-pixel mosaic ccd camera," *Publ. Astro. Soc. Pacific* **104**, pp. 744–751, 1992.
7. T. Usuda *et al.*, "CIAX: Cassegrain instrument auto exchanger for the Subaru telescope," *Proc. SPIE* **4009**, pp. 141–150, 2000.
8. K. Omata *et al.*, "Control of the Subaru telescope instrument exchanger system," *Proc. SPIE* **4009**, pp. 374–385, 2000.
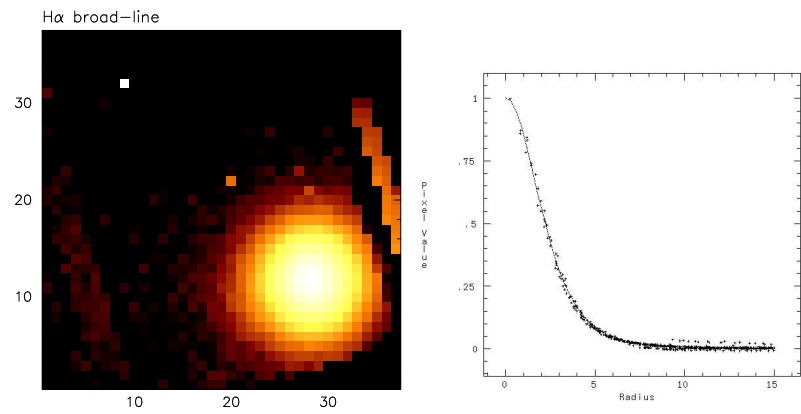
Figure 7. Results with 3DII IFS+Subaru. Seyfert Galaxy NGC 7469. (left): Spatial distribution of *broad* component of Hα line emission. South is up. $3'' = 1$kpc. (right): Fitting result: FWHM=4.4lens= $0''.41$.
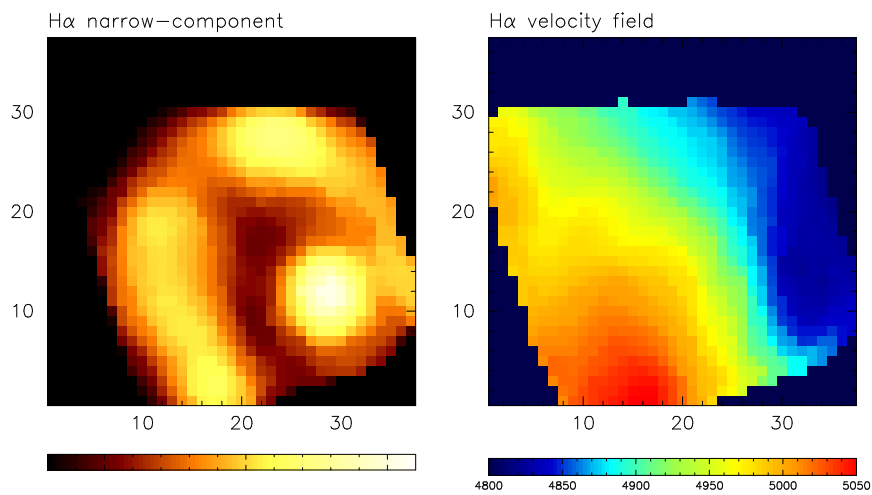

Figure 8. Seyfert Galaxy NGC 7469. (left): Spatial distribution of *narrow* component of Hα line emission. (right): Velocity field of narrow component of Hα line emission.
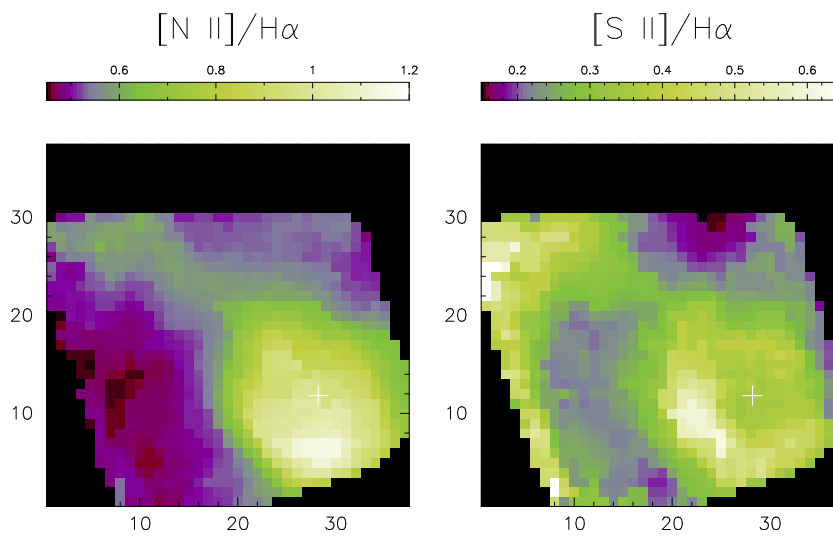
Figure 9. Seyfert Galaxy NGC 7469. While the [NII]/Hα line ratio peak is found to the north of nucleus, the [SII]/Hα peak is found to the west.
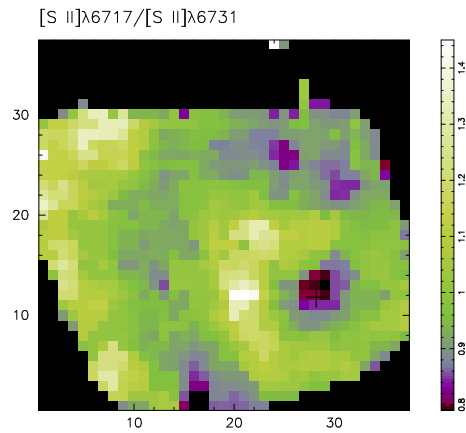

Figure 10. Seyfert Galaxy NGC 7469. [SII] line ratio as an indicator of electron density. White regions have low density.